Fluid inclusion studies on barite from Hutti Gold Mines, Karnataka, India: inferences on late-stage hydrothermal fluid

C. G. Nevin* and H. S. Pandalai

Department of Earth Sciences, Indian Institute of Technology, Mumbai 400 076, India

Late-stage, post-gold mineralization, cavity-filling veins with barite are reported here from the Hutti gold deposit of Karnataka. Large (10–15 cm) to medium (2–5 cm) sized translucent crystals of barite studded with numerous pyrite grains commonly of 1–2 mm size occur in these veins. Monophase and biphase fluid inclusions occur in primary clusters and pseudo-secondary trails in the barite crystals. Microthermometric and laser-Raman studies show that the barite has formed from aqueous fluids of relatively high salinity (14–22 eq. wt% NaCl). Minor Raman-shift peaks of methane are observed in the vapour phase of a few biphase fluid inclusions. Assuming pressure of less than 1 kbar, trapping temperature would be less than 200°C. These post-ore veins at Hutti point to a source of oxidized fluid subsequent to the phase of gold mineralization.

Keywords: Archean gold, barite, Hutti, hydrothermal veins.

BARITE is a common gangue mineral in many carbonate-hosted lead–zinc deposits. Barite is also reported as a gangue mineral in some of the Archean gold deposits[1]. In many of the latter deposits, barite occurs along with post-ore quartz–calcite veins[2]. The present study examines barite veins in the Hutti gold deposit, an Archaean greenstone-hosted mesothermal-gold deposit located in the north-western part of the Hutti–Maski schist belt (Figure 1). Many studies[3–7] have been done on the Hutti–Maski schist belt and the geological setting of the Hutti gold deposit[8]. The schist belt comprises metavolcanics and subordinate metasedimentary rocks and is surrounded by gneisses, granites and granitoids. The metavolcanics include abundant pillowed basalt and thin units of felsic volcanics of dacitic composition. Metasediments include banded haematite quartz, chlorite schists and rare carbonate rocks. At Hutti, gold occurs in nine sub-parallel quartz reefs that trend N10°W and in altered wall rocks that occur beside it. Chloritization, biotitization and carbonatization are the common alterations seen in wall rock metabasalts whereas albitization, sericitation and carbonatization are common alterations in felsic wall rocks. Gold mineralization at Hutti is dated at 2547 Ma (ref. 9).

Gold is present in the Hutti deposit as native gold grains in the shear-hosted laminated fault-fill quartz veins and in altered wall rock besides being present in the lattice of pyrite and arsenopyrite in the altered zone. Calcite is commonly seen along with quartz veins and is particularly common in sheared and altered metabasalts and felsic volcanic rocks. Later quartz–calcite veins cut across the reefs. These are generally oriented in N50°W and run parallel to barren milky quartz veins. These veins are generally devoid of any sulphide or gold mineralization. The late quartz veins clearly cut across the shear-related laminated fault-fill veins that are the gold mineralized reefs at Hutti and are post-ore veins formed by late-stage hydrothermal activity. Barite was not previously reported in any of these veins. Barite was first identified by C. D. Hiremani, Prabhakar Sangurmath and M. L. Patil of Hutti Gold Mines Ltd (HGML) in May 2009 (personal communication). Barite occurs here as a 40 cm thick vein with calcite (Figure 2 *a*). The vein cuts across Strike Reef in the 26th level of the Hutti mines. The vein is oriented N55°W and dips 50° due south and comprises large (10–15 cm) to medium sized (2–5 cm) transparent crystals of barite with well-developed crystal faces (Figure 2 *b*).

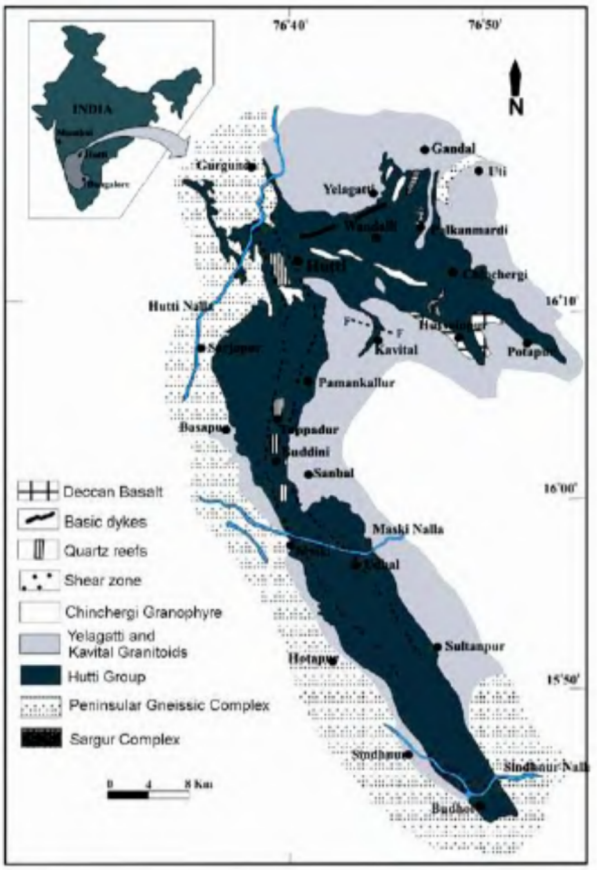

Figure 1. Geological map of Hutti–Maski schist belt, modified after Sundaram *et al.*[19].

*For correspondence. (e-mail: nevincg@iitb.ac.in)

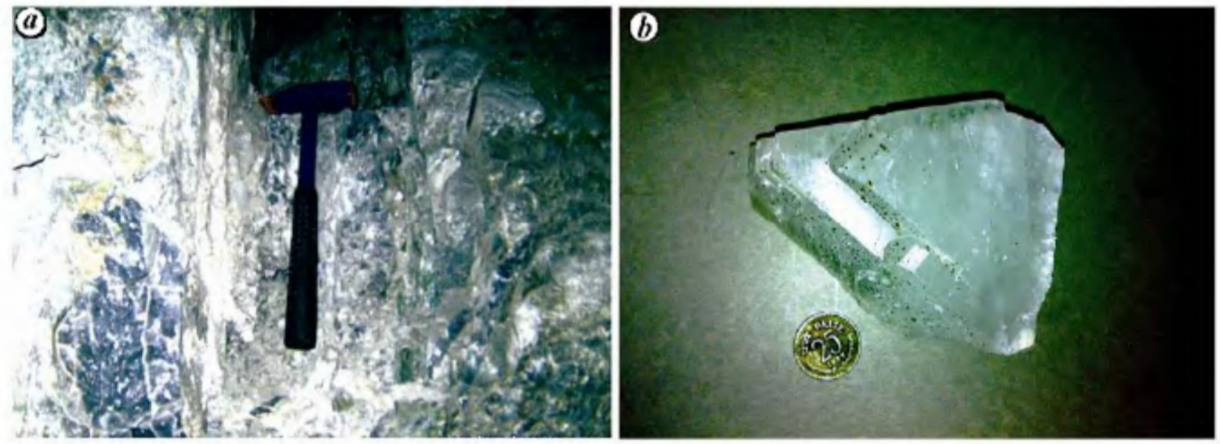

Figure 2. *a*, Barite vein ~40 cm thick that cuts across laminated quartz veins of the Strike Reef. *b*, Transparent to translucent crystalline barite sample collected from the barite vein. Pyrite cubes of 1–2 mm size are seen on the crystal faces.

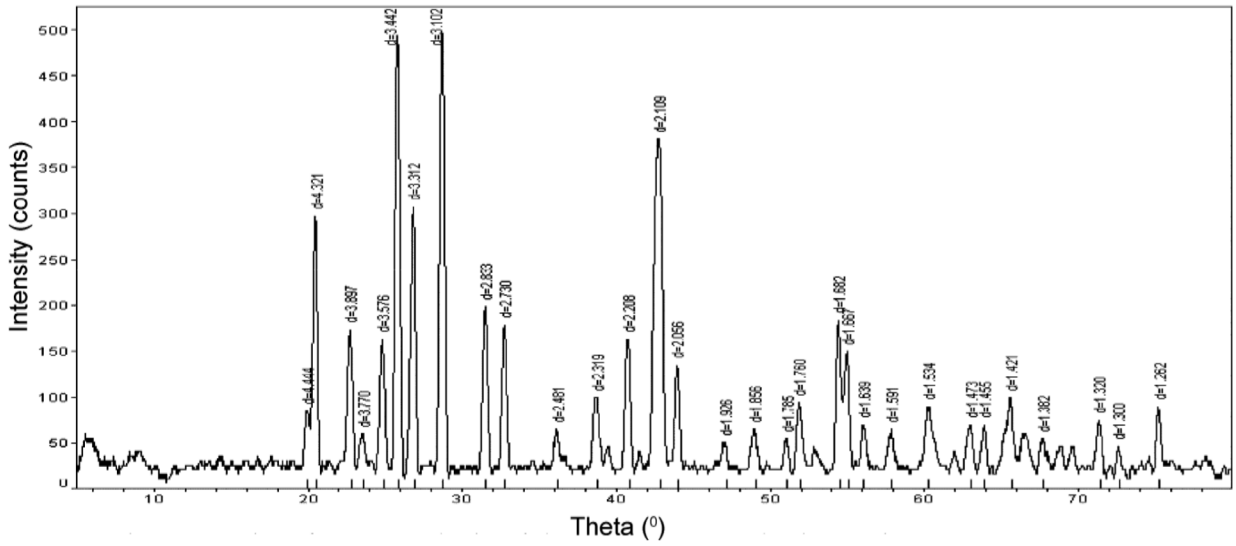

Figure 3. Results of XRD analysis of the sample shows barite peaks.

Small pyrite crystals are commonly embedded on the surfaces of the crystal faces and within the barite crystals. The X-ray diffraction (XRD) and laser-Raman studies confirm the mineralogical identification of the sample (Figures 3 and 4). The well-developed crystalline nature of the veins, the absence of fracturing or effects of deformation at the mesoscopic scale and the cross-cutting nature of the veins relative to the laminated quartz that hosts gold, clearly indicate that the veins represent a cavity filling vein formed during late-stage, post-ore hydrothermal activity at Hutti.

In the present work, the nature of fluid that caused the formation of these barite veins is examined on the basis of fluid inclusion studies that include microthermometry and laser-Raman studies. This study is useful in understanding late-stage hydrothermal fluid activity in the Hutti deposit.

The barite samples from Hutti have a high spatial density of fluid inclusions. These fluid inclusions vary in size from few μm to 300 microns with most of them in the size range of 50–200 microns (Figure 5). Detailed fluid inclusion petrography was carried out in order to distinguish different types of fluid inclusions. Petrography reveals that these are mostly primary and pseudo-secondary fluid inclusions. The fluid inclusions are of monophase and biphase type. Monophase fluid inclusions make up more than 90% of the fluid inclusions present. The primary fluid inclusions occur as isolated and three dimensional clusters (Figure 6 *a*, *c* and *i*) and the pseudo-secondary fluid inclusions occur along trails (Figure 6 *b–d*).

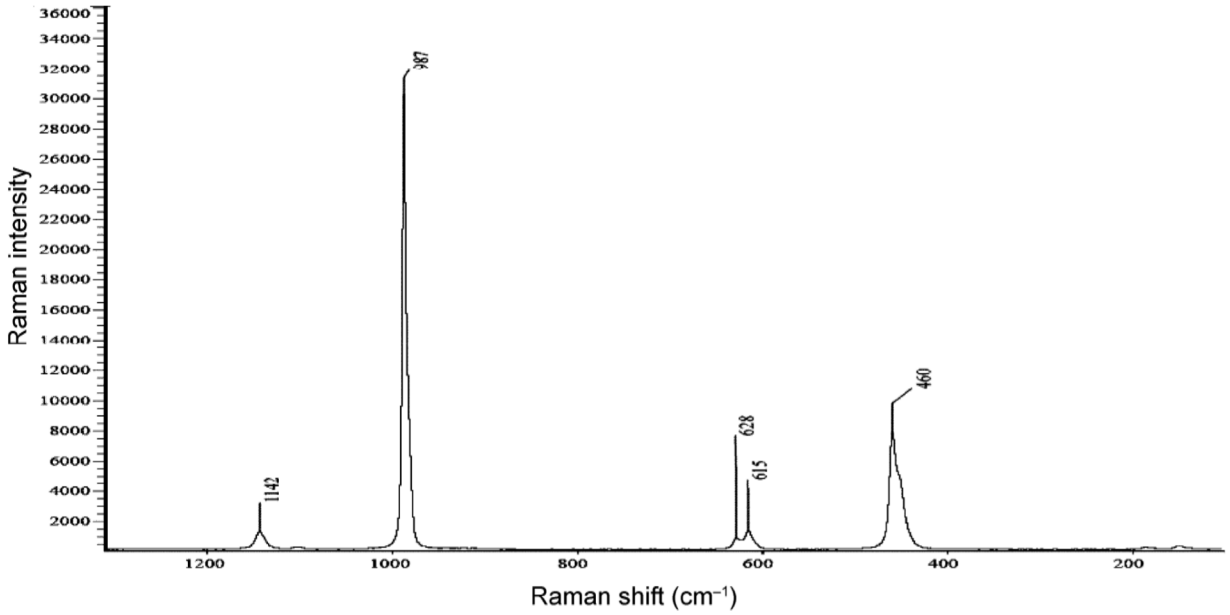

Figure 4. Laser-Raman spectrum of sample showing Raman shifts corresponding to barite.

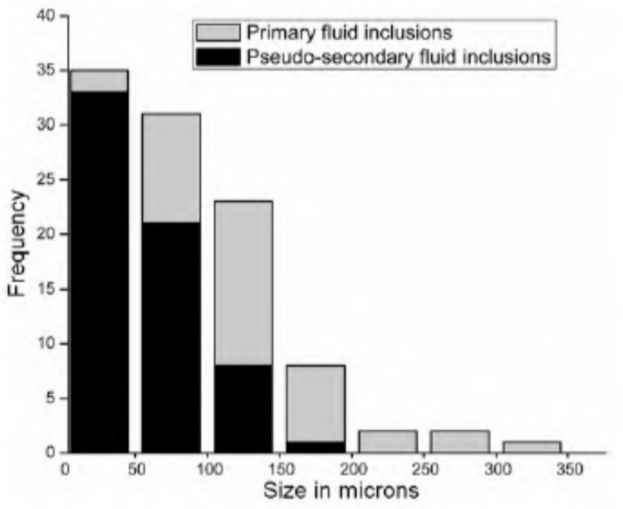

Figure 5. Histogram of size distribution of primary and pseudo-secondary fluid inclusions.

The trails are usually parallel arrays and their parallelism with each other and with cleavage helps to identify them as pseudo-secondary trails.

Based on morphology, the primary fluid inclusions in barite can be classified into two varieties. The first kind occurs as flat fluid inclusions with irregular boundaries. They are of very large size (up to 350 microns, Figure 6 *e*). The second variety consists of elongated and irregular fluid inclusions that have significant size in all three dimensions. Their sizes range from 50 to 250 μm (Figure 6 *f–h*).

Most of the pseudo-secondary trails contain elongated pencil-like fluid inclusions with lengths of 11–200 μm and widths of 8–13 microns (Figure 6 *d*). Some others are negative-crystal shaped or rounded and irregular fluid inclusions (Figure 6 *j–l*). The sizes of these pseudo-secondary inclusions generally vary from 11 to 150 μm.

Based on the number of phases present at room temperature, the primary and pseudo-secondary fluid inclusions are classified into two categories that are termed here as types I and II. Type I fluid inclusions are monophase and the type II are biphase fluid inclusions. Both types I and II fluid inclusions coexist together in close proximity with each other (Figure 6 *l* and *m*). Type II inclusions generally show a liquid to vapour ratio of 90 : 10 (Figure 6 *g*); a few of these show $L : V$ ratios as low as 40 : 60 (Figure 6 *h*). The fluid inclusions with low $L : V$ ratios may have undergone leakage during cooling. Some primary and pseudo-secondary fluid inclusions show evidence of necking (Figure 6 *n*). Polyphase inclusions with daughter crystals are absent in the barite samples.

In order to understand the composition of the fluid, microthermometric studies and laser Raman studies were conducted on the fluid inclusions in the barite samples.

Heating and freezing tests were conducted on cleaved chips using Linkam THMSG 600 stage attached to Leitz Ortholux II Pol-BK microscope with 50× objective. Cleaved chips were used because barite can undergo thermal and mechanical damage during polished wafer preparation[10–13]. Heating and freezing studies were carried out on separate cleaved chips in order to eliminate errors due to freeze-stretching of the inclusions[10,14] that is commonly seen in fluid inclusions in barite.

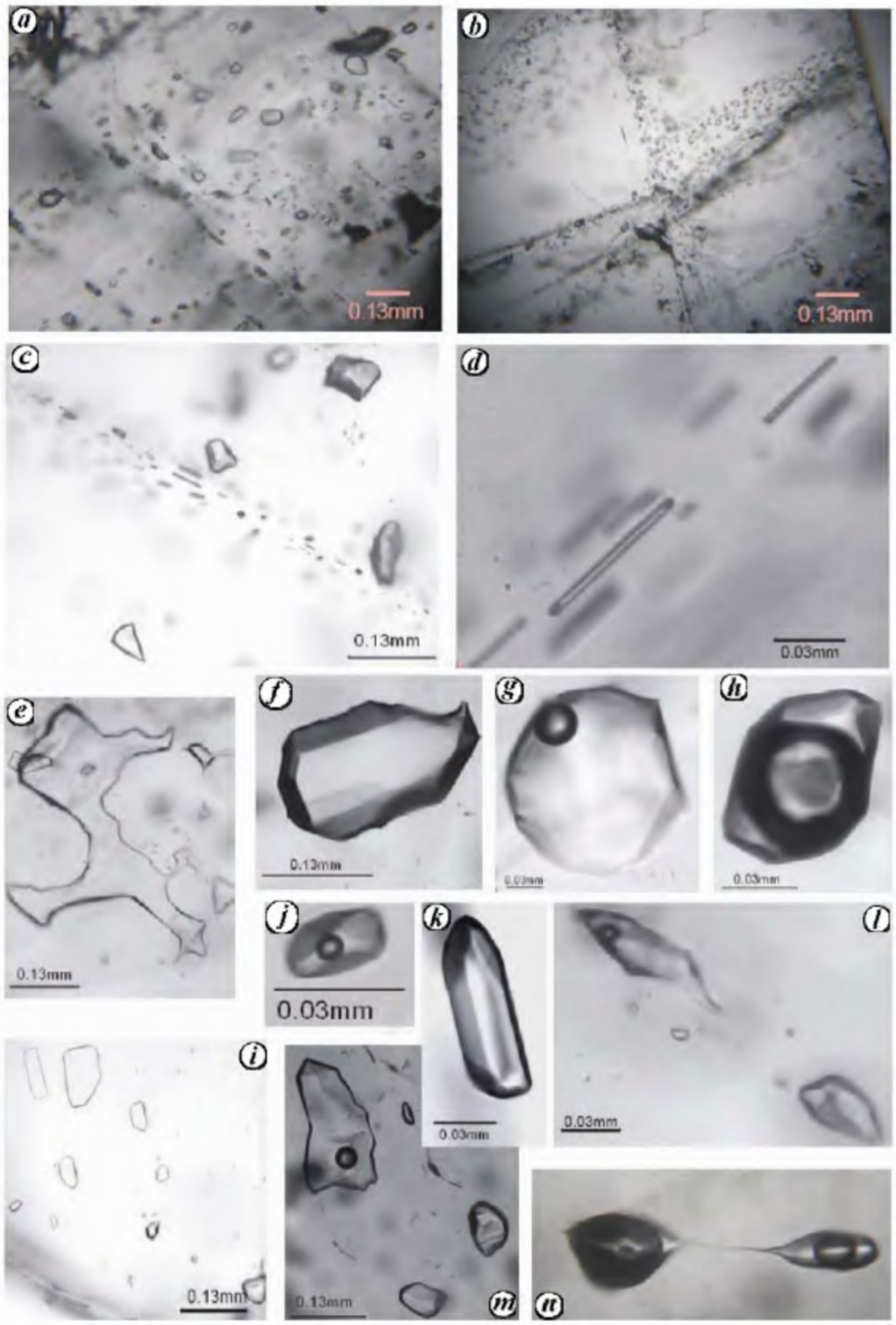

Figure 6. ***a***, Three-dimensional array of primary fluid inclusions. ***b***, Trails of pseudo-secondary fluid inclusions. ***c***, Primary, isolated monophase fluid inclusions and trails of pseudo-secondary monophase fluid inclusions. ***d***, Pencil shaped pseudo-secondary monophase fluid inclusions. ***e***, Flat, primary, monophase fluid inclusions with irregular boundaries. ***f***, Primary monophase fluid inclusions of elongated type. ***g***, Primary biphase fluid inclusions with $L:V$ ratio of 90 : 10. ***h***, Primary biphase fluid inclusions with a low $L:V$ ratio. ***i***, Three-dimensional array of primary monophase flat fluid inclusions. ***j***, Pseudo-secondary biphase fluid inclusions. ***k***, Elongated negative crystal cavity pseudo-secondary fluid inclusions. ***l***, Pseudo-secondary fluid inclusion trails that show coexistence of monophase and biphase fluid inclusions. ***m***, Coexistence of primary biphase and monophase inclusions in three-dimensional array. ***n***, Necked biphase fluid inclusion.

Most of the type I (monophase) fluid inclusions do not show any bubble nucleation during cooling but total freezing occurs between –80°C and –45°C with a honey yellowish coloured solid phase. Due to the stretching of inclusions during solidification, many of the inclusions develop minor fractures on their sides. These fractures are observable in the frozen state of the fluid inclusion. The fractures cannot be seen after ice-melting and appear to close and heal during re-heating. Upon re-heating, first ice-melting is observed between –47°C and –32°C and final ice melting is observed between –19°C and –6°C. On freezing and re-heating, a few monophase fluid inclusions develop bubbles that persist at room temperature. This is probably due to leakage of fluid through fractures developed on freezing. A schematic diagram of freezing observations on types I and II fluid inclusions is given in Figure 7.

In the case of type II, biphase fluid inclusions, total freezing occurs at –65°C to –43°C. First ice-melting is observed between –30°C and –45°C. Figure 8 *a* shows histograms of eutectic temperatures of both types I and II fluid inclusions which are inferred to be aqueous solutions of several electrolytes.

Final ice-melting in type II fluid inclusions occurs between –6°C and –18°C. In primary biphase (type II) fluid inclusions, last ice-melting varies from –6°C to –14°C and in pseudo-secondary fluid inclusions, it ranges from –14°C to –18°C. The bubble reappears immediately on final melting of ice in all cases.

For the purpose of comparing final ice melting temperatures of primary and pseudo-secondary types I and II fluid inclusions, histograms were constructed (Figure 8 *b*). The final ice-melting temperatures of type I primary fluid inclusions varies between –10°C and –14°C with maxima between –10°C and –12°C. The type I pseudo-secondary fluid inclusions show final ice-melting temperature that varies from –7°C and –19°C with a maximum between –18°C and –19°C. The maximum values of primary type II fluid inclusions lie between –12°C and –14°C whereas for pseudo-secondary type II fluid inclusions, the maximum ranges between –17°C and –18°C. In both types I and II inclusions, the pseudo-secondary fluid inclusions show a slightly but distinctly higher value of salinity.

The equivalent wt% NaCl of the dissolved salts in types I and II fluid inclusions are calculated[15] and the salinity values vary from 10 to 22 eq. wt% NaCl. Figure 8 *c* shows the salinity of types I and II primary and pseudo-secondary fluid inclusions. The primary biphase fluid inclusions have salinity largely in the range of 16–18 eq. wt% NaCl and the primary monophase fluid inclusions have salinity of 14–18 eq. wt% NaCl. The pseudo-secondary biphase fluid inclusions show a spread of values between 18 and 22 eq. wt% NaCl and pseudo-secondary monophase fluid inclusions have salinities in the range of 16–22 eq. wt% NaCl. Although the salinities of primary and pseudo-secondary fluid inclusions largely overlap in the range of 14 and 18 eq. wt% NaCl, pseudo-secondary biphase fluid inclusions show salinities that extend up to 22 eq. wt% NaCl while some primary biphase fluid inclusions and pseudo-secondary monophase fluid inclusions show values as low as 10 eq. wt% NaCl. The salinity of pseudo-secondary biphase and monophase fluid inclusions is slightly higher than that of primary fluid inclusions.

The lack of a vapour phase in the monophase fluid inclusions may be due to leakage of the vapour after the fluid inclusions are cooled down to low temperatures. The continued inability of most of these fluid inclusions to nucleate a vapour bubble during cooling is intriguing and may be due to reduction in fluid inclusion volume on account of the low strength of the host. This conclusion is also supported by the observation that in the case of biphase fluid inclusions there is no appreciable change in bubble volume upon cooling. The low strength of the host barite, also accounts for the development of fractures in monophase fluid inclusions during freezing. These fluid inclusions are unable to contain the pressure developed within them during freeze-stretching leading to development of fractures.

The salinity values of monophase and biphase fluid inclusions range between 14 and 22 eq. wt% range. This fact as well as their close proximity to each other in three-dimensional arrays and in pseudo-secondary trails indicates that they have been derived from the same fluids.

Most biphase (type II) fluid inclusions show a constant $L : V$ ratio (90 : 10) irrespective of whether they belong to

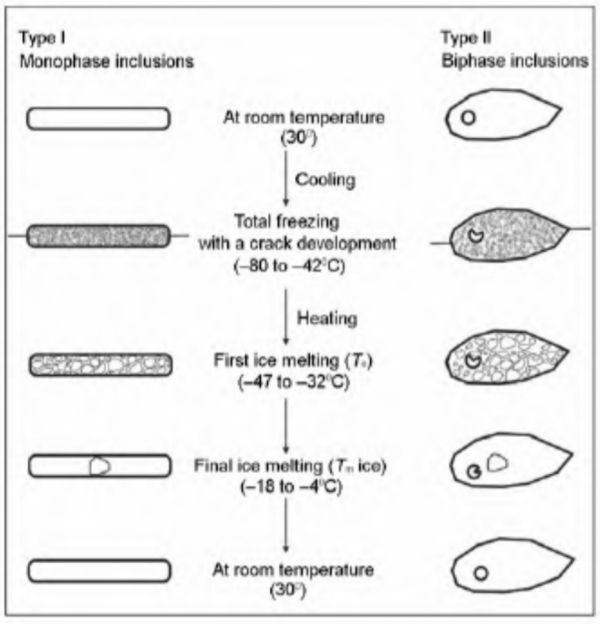

Figure 7. Schematic diagram of changes in monophase and biphase fluid inclusions during freezing studies.

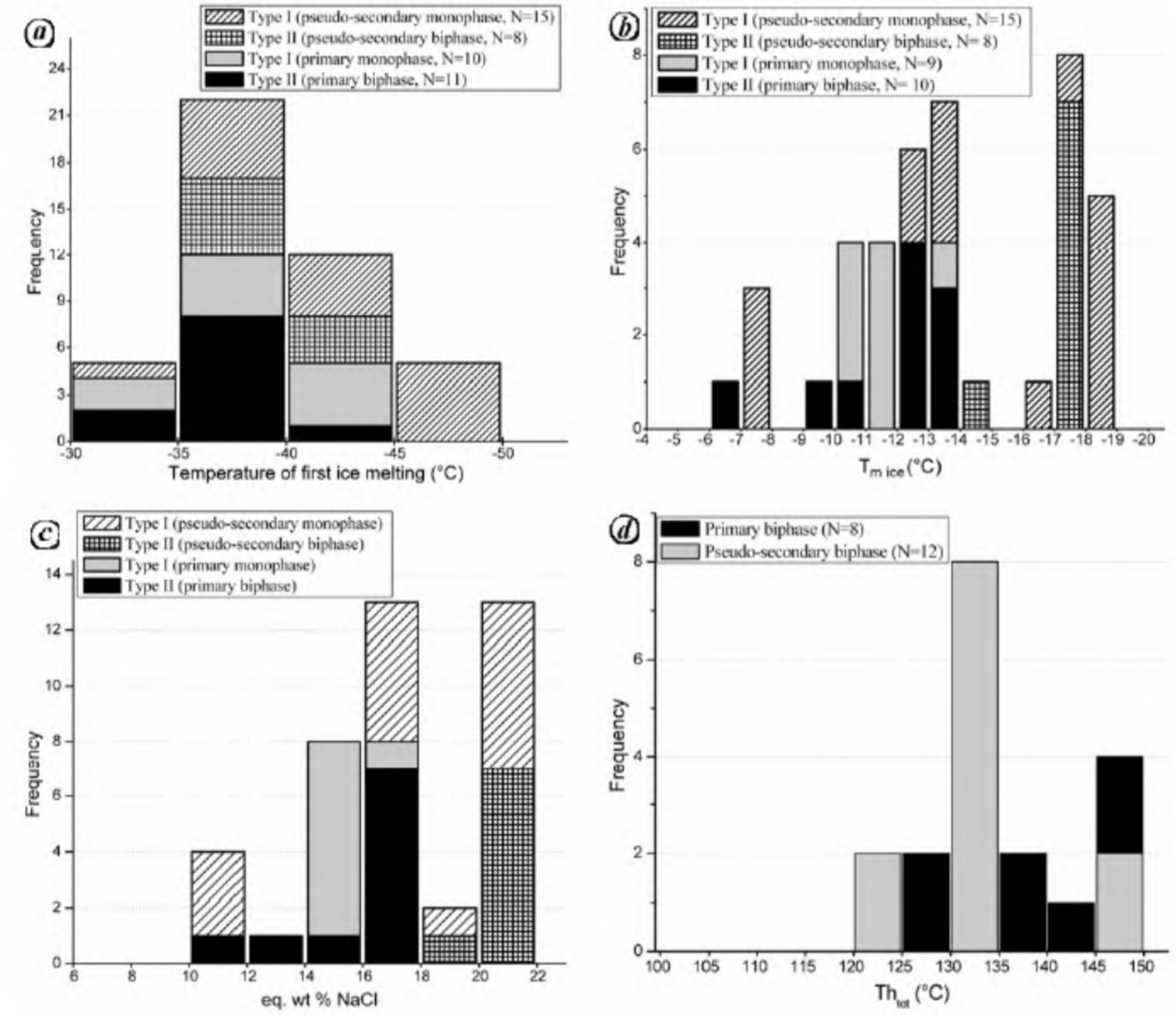

Figure 8. Histogram of temperatures of phase-changes during microthermometric runs and computed salinities. ***a***, First ice-melting temperature. ***b***, Final ice-melting temperature ($T_{m\ ice}$). ***c***, Salinity (equivalent wt% NaCl) of primary and pseudo-secondary monophase and biphase fluid inclusions. ***d***, Homogenization temperature (Th_{tot}) of biphase primary and pseudo-secondary fluid inclusions.

the primary or pseudo-secondary category. Due to stretching during over-heating, barite is not a good mineral for studying homogenization temperatures[11,15]. Nevertheless, homogenization temperatures were measured carefully on selected fluid inclusions of the Hutti barite in several cleaved chips. The histograms of total homogenization temperature of the primary and pseudo-secondary type II fluid inclusions are shown in Figure 8 *d*. The primary biphase inclusions show a range of homogenization temperature that varies from 125°C to 150°C with most values between 135°C and 150°C. The mode of temperature of homogenization of pseudo-secondary biphase fluid inclusions is between 130°C and 135°C. All the inclusions show transition from liquid–vapour to liquid phase. The primary biphase fluid inclusions show a slightly but distinctly higher mode of temperatures of homogenization in comparison to the pseudo-secondary fluid inclusions. The summary of microthermometric data is given in Table 1.

Laser-Raman studies on type I inclusions show that the fluid inclusions are aqueous in nature (Figure 9) although a few type II primary inclusions show the presence of minor CH_4 in the vapour phase (Figure 9). The pseudo-secondary biphase inclusions could not be analysed because of rapid movement of the vapour bubble.

The barite vein at Hutti is a cavity-filling vein. The undeformed nature of the vein and the occurrence of barite and calcite in the form of well-preserved crystals and the

Table 1. Microthermometric data from different types of fluid inclusions

		Primary		Pseudo-secondary	
		Type I	Type II	Type I	Type II
First ice melting (°C)	Range	–30 to –45	–30 to –45	–30 to –50	–35 to –45
	Mode	–35 to –45	–35 to –40	–35 to –40 and –45 to –50	–35 to –40
Final ice melting (°C)	Range	–10 to –14	–6 to –14	–7 to –19	–4 to –18
	Mode	–10 to –12	–12 to –14	–18 to –19	–17 to –18
Homogenization temperature (°C)	Range		125 to150		125 to150
	Mode		135 to150		130 to135
Salinity (eq. wt% NaCl)	Range	14 to18	10 to18	10 to 22	18 to 22
	Mode	14 to16	16 to18	20 to 22 and 16 to18	20 to 22

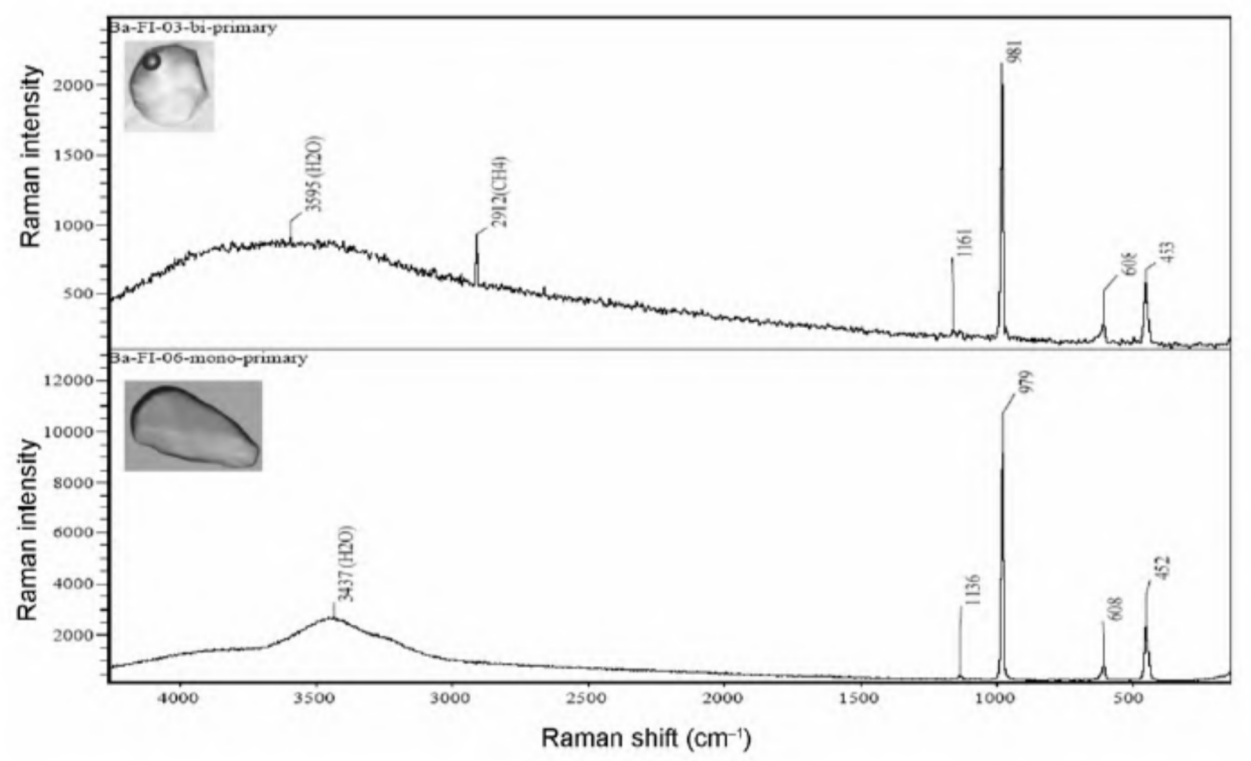

Figure 9. Laser-Raman spectrographs of a biphase fluid inclusion showing peaks of H_2O and CH_4 in the vapour phase and a monophase fluid inclusion showing only H_2O peak.

cross-cutting relation of the vein with the laminated quartz of Strike Reef indicate that the vein is the result of late-stage hydrothermal activity at Hutti. The large-sized fluid inclusions and their near-perfect negative crystal outline also indicate that the barite vein has not undergone deformation after its formation. Microthermometric and laser-Raman studies show that the barite has formed from aqueous fluids of relatively high salinity. The salinity of the fluid varies from 10 to 22 eq. wt% NaCl but most values cluster between 14 and 22 eq. wt% NaCl. In contrast, the laminated quartz veins that host gold have formed from fluids of low salinity that generally range between 0 and 14 eq. wt.% NaCl[8].

The temperature of homogenization of the biphase fluid inclusions in barite is less than 150°C. The slight variation in salinity and homogenization temperature between primary and pseudo-secondary fluid inclusions is within the range of experimental error. A value of 1.0 to 1.7 kbar is estimated as the pressure for the lower end of greenschist facies metamorphism at Hutti[8,16,17]. Assuming that the barite veins formed at a late stage, it is estimated that pressure is less than 1 kbar. At 1 kbar, trapping temperature would be less than 200°C. The post-ore barite veins at Hutti indicate a source of relatively oxidized fluid subsequent to the phase of gold mineralization. Oxidizing fluids related to felsic magmatism have

been considered as an important possible source for such barite vein[18]. The source of Ba and the oxidized fluids that led to precipitation of post-ore barite at Hutti needs further investigation.

1. Michibayashi, K., Two-phase syntectonic gold mineralization and barite remobilization within the main ore body of the Golden Giant mine, Hemlo, Ontario, Canada. *Ore Geol. Rev.*, 1995, **10**, 31–50.
2. Robert, F. and Poulsen, K. H., World-class Archaean gold deposits in Canada: an overview. *Aust. J. Earth Sci.*, 1997, **44**, 329–351.
3. Roy, A., Polyphase folding deformation in the Hutti–Maski schist belt, Karnataka. *J. Geol. Soc. India*, 1979, **20**, 598–607.
4. Roy, A., The geology of gold mineralization at Hutti in Hutti-Maski schist belt. *Indian Minerals*, 1991, **45**, 229–250.
5. Vasudev, V. N. and Chadwick, B., Lithology and structure of the auriferous Hutti schist belt, Northern Karnataka: Implications for neoarchean oblique convergence in the Dharwar craton, South India. *J. Geol. Soc. India*, 2008, **71**, 239–256.
6. Biswas, S. K., Gold mineralization in the Hutti–Maski greenstone belt, Karnataka, India. *Indian Minerals*, 1990, **44**, 1–14.
7. Riyaz Ullah, M. S., Pathan, A. and Maaskant, P., The characterization of metamorphic facies of metabasalts of Hutti greenstone belt. *J. Geol. Soc. India*, 1996, **47**, 547–554.
8. Pandalai, H. S., Jadhav, G. N., Biju Mathew, Panchapakesan, V., Raju, K. K. and Patil, M. L., Dissolution channels in quartz and the role of pressure changes in gold and sulphide deposition in the Archaean, greenstone-hosted, Hutti gold deposit, Karnataka, India. *Min. Dep.*, 2003, **38**, 597–624.
9. Sarma, D. S., McNaughton, N., Fletcher, I. R., Groves, D. I., Mohan, M. R. and Balaram, V., Timing of gold mineralization in the Hutti gold deposit, Dharwar Craton, South India. *Econ. Geol.*, 2008, **103**, 1715–1727.
10. Ulrich, R. M., and Bodnar, R. J., Systematics of stretching of fluid inclusions II: Barite at 1 ATM confining pressures. *Econ. Geol.*, 1988, **88**, 1037–1046.
11. Roedder, E. and Skinner, B. J., Experimental evidence that fluid inclusions do not leak. *Econ. Geol.*, 1968, **63**, 715–730.
12. Faiziev, A. R. and Alidovov, B. A., Thermometry of minerals with perfect cleavage. *Soviet Geol. Geophys.*, 1976, **17**, 118–121.
13. Lawler, J. P. and Crawford, M. L., Stretching of fluid inclusions resulting from low-temperature microthermometric technique. *Econ. Geol.*, 1983, **78**, 527–529.
14. Bodnar, R. J. and Bethke, P. M., Systematics of stretching of fluid inclusions I: Fluorite and sphalerite at 1 atmosphere confining pressure. *Econ. Geol.*, 1984, **79**, 147–161.
15. Bodnar, R. J. and Vityk, M. O., Interpretation of microthermometric data for H_2O–NaCl fluid inclusions. In *Fluid Inclusions in Minerals: Methods and Applications* (eds De Vivo, B. and Frezzotti, M. L.), 1994, pp. 117–130.
16. Pal, N. and Mishra, B., Alteration geochemistry and fluid inclusion characteristics of the greenstone hosted gold deposit at Hutti, eastern Dharwar craton, India. *Min. Dep.*, 2002, **37**, 722–736.
17. Mishra, B. and Pal, N., Metamorphism, fluid flux, and fluid evolution relative to gold mineralization in the Hutti–Maski greenstone belt, eastern Dharwar craton, India. *Econ. Geol.*, 2008, **103**, 801–827.
18. Cameroon, E. M. and Hattori, K., Archaean gold mineralization and oxidized hydrothermal fluids. *Econ. Geol.*, 1987, **82**, 1177–1191.
19. Sundaram, V., Kumaran, C. J., Dorai Swamy, K., Lakshmana, B. K., Ananthanarayana, R. and Srikantia, S. V., Geological Survey of India quoted in Srikantia S. V., Geology of the Hutti–Maski greenstone belt. In *Hutti Gold Mine: Into the 21st Century* (eds Curtis, L. C. and Radhakrishna, B. P.), Geological Society of India, 1995, pp. 8–27.

ACKNOWLEDGEMENTS. We acknowledge the continued support extended to us by the Hutti Gold Mines Company Limited (HGML) over several years that has helped in collection of samples and in understanding of the Hutti deposit. All geologists of the exploration and Geology Department of the HGML are thanked for their kind cooperation. We thank Mr C. D. Hiremani, Dr Prabhakar Sangurmath and Dr M. L. Patil, General Manager, HGML for information on the barite veins, their support and encouragement.

Received 30 September 2009; accepted 3 March 2010

Molecular characterization of chikungunya virus in febrile patients from central Kerala by RT-PCR assay

P. Venkatachalam[1,*], M. B. Mohamed Sathik[2], Prasad P. Mani[3], Valsala Kumari[3], T. Saha[2] and James Jacob[2]

[1]Department of Biotechnology, Periyar University, Salem 636 011, India
[2]Advanced Centre for Molecular Biology and Biotechnology, Rubber Research Institute of India, Rubber Board P.O., Kottayam 686 009, India
[3]District Hospital, Kottayam 686 001, India

Chikungunya fever, caused by infection with mosquito-borne alphavirus is an acute nonfatal illness characterized by fever, rash, myalgia, arthralgia and sometimes inflammatory arthritis. During 2007, central Kerala experienced a chikungunya fever epidemic of unprecedented magnitude. There were unusual skin manifestations like peeling of scrotal skin, non-healing ulcer and soft tissue necrosis. cDNA copy of a portion of the viral genome was synthesized in a reverse transcription reaction in the presence of specific primers for the E1 region of the S27 African strain of chikungunya virus (CHIKV) followed by polymerase chain reaction (PCR) amplification. Among 23 patients sampled, nine cases were found CHIKV positive. In PCR confirmed cases, the knees and ankles were the joints commonly affected. Our results suggest that the viraemia could be detected in blood during the first seven days of illness only. Three mismatches observed in the DNA sequence indicate that the virus may be a deviant of the African prototype.

Keywords: Blood samples *E1* gene, chikungunya virus, polymerase chain reaction.

*For correspondence. (e-mail: pvenkat67@yahoo.com)